



# Spin–orbit coupling in $I \cdot CO_2$ and $I \cdot OCS$ van der Waals complexes: beyond the pseudo-diatomic approximation

Andrei Sanov<sup>1</sup>, James Faeder, Robert Parson, W. Carl Lineberger<sup>\*</sup>

*JILA, National Institute of Standards and Technology and University of Colorado, and Department of Chemistry and Biochemistry, University of Colorado, Boulder, CO 80309-0440, USA*

Received 4 March 1999; in final form 14 July 1999

## Abstract

We investigate theoretically the electronic structure of  $I \cdot CO_2$  and  $I \cdot OCS$  van der Waals complexes including spin–orbit interaction. For the T-shaped geometry of  $I \cdot CO_2$ , we calculate the potentials using a fully polyatomic treatment and compare the results to the widely used pseudo-diatomic approximation. The latter becomes increasingly invalid at  $I-CO_2$  distances shorter than 4 Å. We calculate the potentials of linear  $I \cdot SCO$  and  $I \cdot OCS$ , and analyze the zero-order electronic structure of nonlinear  $I \cdot OCS$ . We also discuss the validity of treating the spin–orbit interaction in  $I \cdot CO_2$  and  $I \cdot OCS$  as an atomic property of iodine and find this approximation justified at characteristic van der Waals distances. © 1999 Elsevier Science B.V. All rights reserved.

## 1. Introduction

Studies of spectroscopy and dynamics of solvated halide and dihalide anions have yielded a wealth of information about intermolecular interactions involving both charged and neutral, open- and closed-shell species. The interpretation of experimental results and understanding of photochemistry of solvated species relies on the modeling of intermolecular interaction potentials. The neutral halogen clusters, such as  $I \cdot X$  (where  $X$  is a closed-shell solvent), present special challenges to theoretical calculations due to their open-shell electronic structure and strong spin–orbit coupling that exceeds the van der Waals

bonding. In this Letter, we explore aspects of the  $I \cdot CO_2$  electronic structure that have not been adequately addressed previously, and investigate for the first time the electronic structure of  $I \cdot OCS$ .

The  $I \cdot CO_2$  van der Waals complex has been the subject of several experimental and theoretical studies [1–5]. Of particular interest is the T-shaped  $C_{2v}$  geometry of the complex, as it is this geometry that is accessed in the photodetachment of the  $I^- \cdot CO_2$  anion [1–3]. Previous theoretical studies of the  $C_{2v}$  complex relied on a pseudo-diatomic approximation [3–5], explicitly treating  $CO_2$  as a rare-gas atom. This approximation reduces the complex to a ‘diatomic’ system analogous to many systems studied previously, e.g., metal–rare-gas complexes [6–8] and rare-gas halides [9–12]. In what follows, we explore the limitations of the pseudo-diatomic approximation by comparing the potentials calculated using both the pseudo-diatomic and truly polyatomic descriptions.

<sup>\*</sup> Corresponding author. Fax: +1-303-492-8994; e-mail: wcl@jila.colorado.edu

<sup>1</sup> Present address: Department of Chemistry, The University of Arizona, Tucson, AZ 85721, USA.

In contrast to  $I \cdot CO_2$ , the electronic structure of  $I \cdot OCS$  has remained unexplored by both the experiment and theory, and no photodetachment studies have been reported for  $I^- \cdot OCS$ . Our recent calculations showed that the global potential minimum of the anion corresponds to a linear  $I^- \cdot SCO$  charge-dipole-bound geometry with an I–S distance of 3.6 Å and a dissociation energy of 220 meV [13]. The linear  $I^- \cdot OCS$  configuration is repulsive, whereas a shoulder on the potential energy surface of nonlinear  $I^- \cdot OCS$  corresponds to a roughly T-shaped charge-quadrupole-bound geometry [13]. Here, we calculate the electronic structure of linear  $I \cdot OCS$  and  $I \cdot SCO$ . We also analyze the zero-order electronic structure of nonlinear  $I \cdot OCS$ .

For the treatment of spin–orbit interactions, we rely on the physical model of Dunning and Hay, originally developed for diatomic rare-gas halides [9–12]. This model was applied previously to the pseudo-diatom treatment of  $I \cdot CO_2$  [1,3–5]; we extend it to a truly polyatomic nonlinear case. The spin–orbit interaction within the complex is treated as an atomic property of iodine. We discuss the validity of this treatment at various complex geometries.

## 2. Method

For both  $I \cdot CO_2$  and  $I \cdot OCS$ , we first calculate zero-order electronic potentials neglecting the spin–orbit interaction. In the case of  $I \cdot CO_2$ , the zero-order potentials are calculated using both the pseudo-diatom and polyatomic descriptions of the complex. Then, we introduce the spin–orbit coupling, which is treated as an atomic property of iodine so that the corresponding part of the Hamiltonian is considered independent of the complex geometry. While this approximation is reasonable at the I– $CO_2$  and I–OCS distances characteristic of van der Waals interactions, it becomes invalid at shorter separations. We analyze its breakdown by considering the spin density distributions.

The zero-order ab initio calculations are carried out with Gaussian 94 [14], using Becke's three-parameter density-functional method [15] with unrestricted spin and the correlation functional of Lee, Yang, and Parr [16] (B3LYP). For iodine, we use the

relativistic effective core potential (ECP) of Hay and Wadt [17], combined with a double-zeta valence basis set (LanL2DZ). We augment the basis with uncontracted s and p diffuse functions (exponents 0.0569 and 0.0330, respectively) and d and f polarization functions (exponents 0.292 and 0.441, respectively) [18]. For C, O, and S, Dunning's aug-cc-pVDZ all-electron basis sets [19–21] are used. In calculations on neutral complexes, the  $CO_2$  and OCS moieties are kept frozen at the optimized linear geometries of isolated molecules ( $R_{CO} = 1.17$  Å in  $CO_2$ ;  $R_{CO} = 1.16$  Å and  $R_{CS} = 1.58$  Å in OCS). For ionic species, full geometry optimizations are carried out. The zero-point vibrational energies are not included.

## 3. $I \cdot CO_2$ van der Waals complex

In this section, we compare the potential energy curves of the  $I \cdot CO_2$   $C_{2v}$  complex obtained by the polyatomic and pseudo-diatom treatments. In both approaches, we first calculate the zero-order elec-

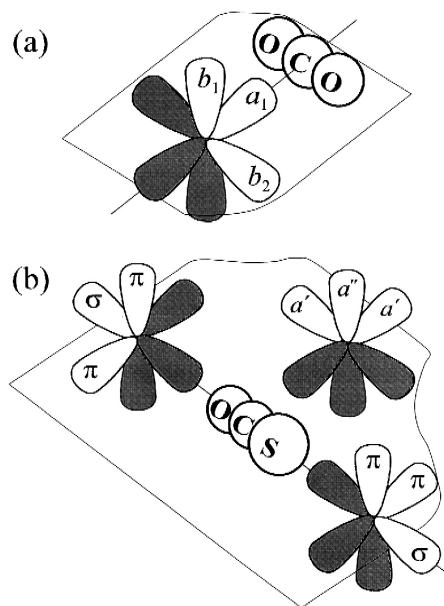


Fig. 1. (a) Orientations of the three 5p orbitals of the I atom in the  $C_{2v}$   $I \cdot CO_2$  complex, corresponding to the  $a_1$ ,  $b_1$ , and  $b_2$  molecular orbitals of the complex. (b) The I 5p orbitals in the  $I \cdot OCS$  complex, corresponding to three different positions of the I atom relative to OCS.

tronic potentials of the complex by neglecting the spin–orbit interaction, then introduce the spin–orbit coupling and rediagonalize the Hamiltonian matrix.

In the zero-order picture, five electrons occupy the three 5p orbitals of the I atom [shown in Fig. 1a, corresponding to the  $a_1$ ,  $b_1$ , and  $b_2$  molecular orbitals of the  $C_{2v}$  complex. Depending on which of these orbitals is half-filled, there are three distinct electronic states:  ${}^2A_1$ ,  ${}^2B_1$ , and  ${}^2B_2$ , respectively. In the pseudo-diatomic approximation, the  ${}^2A_1$  state transforms into a  ${}^2\Sigma$  state, while the  ${}^2B_1$ , and  ${}^2B_2$  states (non-degenerate in the polyatomic treatment) both correspond to a degenerate  ${}^2\Pi$  state. As will be shown shortly, this artificially imposed degeneracy leads to nontrivial electronic structure effects.

Fig. 2a shows the ab initio potential energy curves for the  ${}^2A_1$ ,  ${}^2B_1$ , and  ${}^2B_2$  states. To evaluate the

quality of these potentials, we compare the results of similar calculations on the closed-shell  $I^- \cdot CO_2$  anion to available experimental and theoretical data [1–5]. In  $I^- \cdot CO_2$ , the  $CO_2$  moiety is bent. Our calculations predict an equilibrium OCO angle of  $174.3^\circ$  and an I–C distance of  $3.65 \text{ \AA}$ , in agreement with previous results ( $174.5^\circ \pm 1.5^\circ$  and  $3.77 \text{ \AA}$ ) [1–5]. Excellent agreement with the experiment is achieved in comparing the vertical electron detachment energy (VDE) of  $I^- \cdot CO_2$  to the electron affinity (EA) of the I atom. The VDE of  $I^- \cdot CO_2$  is calculated to exceed the EA of I by 175 meV, compared to the observed 172 meV shift of the photoelectron spectrum of  $I^- \cdot CO_2$  relative to that of bare  $I^-$  [1,2].

The hole in one of the iodine p orbitals is associated with a positive quadrupole moment aligned

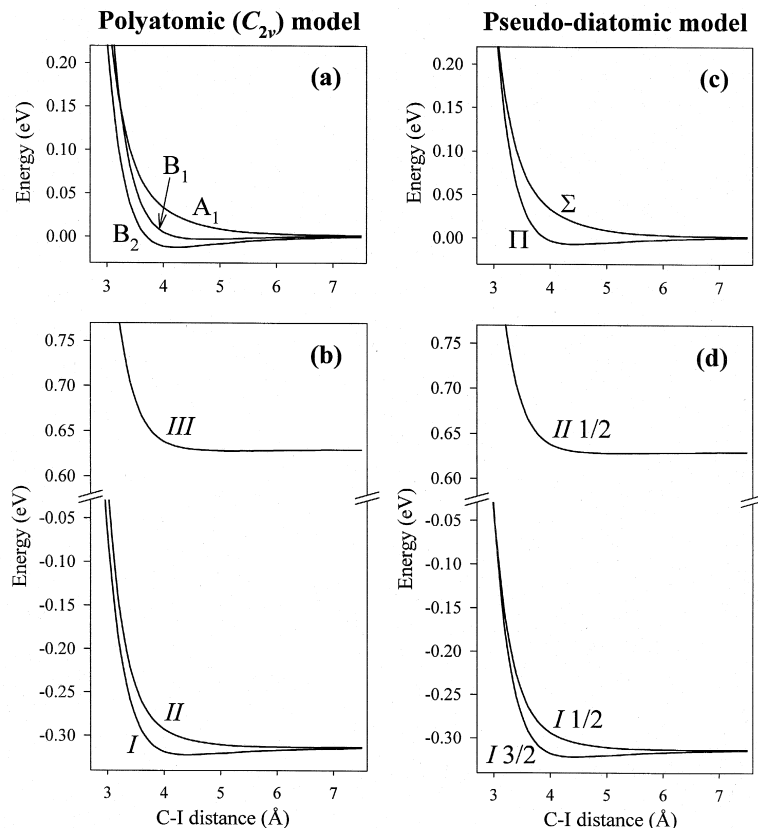


Fig. 2. Calculated potentials energy curves of the  $C_{2v}$   $I \cdot CO_2$  complex: (a) the  $C_{2v}$  potentials corresponding to the  $A_1$ ,  $B_1$ , and  $B_2$  zero-order electronic states; (b) the  $C_{2v}$  potentials including spin–orbit interaction; (c) zero-order potentials calculated using the pseudo-diatomic approximation; and (d) pseudo-diatomic potentials including spin–orbit coupling.

along this orbital. As in the pseudo-diatomic analysis [4,5], the energetic order of the  $A_1$ ,  $B_1$ , and  $B_2$  states is determined by the interaction of this quadrupole with  $\text{CO}_2$ . The  $A_1$  state is destabilized by interaction of the hole with the slightly positive charge on the carbon atom. In the  $B_2$  state, the positive quadrupole associated with the hole leads to an attractive interaction with the negative quadrupole moment of  $\text{CO}_2$ , whereas in the  $b_1$ , out-of-plane orientation, the interaction of the hole with  $\text{CO}_2$  is minimized. The energetic order of the  $B_2$ ,  $B_1$ , and  $A_1$  states observed in Fig. 2a at not too short distances agrees with this qualitative analysis. At short I–C distances, the state ordering changes because in the  $A_1$  state there is less repulsion between the electrons on  $\text{CO}_2$  and the single electron in the  $a_1$  orbital.

To account for the spin–orbit interaction, we modify the physical model developed by Dunning and Hay for diatomic rare-gas halides [9–12], extending it to nonlinear polyatomics. Following Dunning and Hay [9–12], we treat the spin–orbit interaction within the complex as an atomic property of iodine. This approximation leads to the following explicit assumptions: (1) the spin–orbit coupling matrix elements are independent of the geometry of the complex; (2) these elements are the same for each pair of the zero-order electronic states; and (3) they can be evaluated from the isolated I-atom limit.

The electronic Hamiltonian matrix, including spin–orbit coupling, is expressed as:

$$H(r) = \begin{bmatrix} A_1(r) & \lambda & \lambda \\ \lambda & B_1(r) & \lambda \\ \lambda & \lambda & B_2(r) \end{bmatrix}, \quad (1)$$

where  $r$  is the I–C distance;  $A_1(r)$ ,  $B_1(r)$ ,  $B_2(r)$  are the  ${}^2A_1$ ,  ${}^2B_1$ , and  ${}^2B_2$  zero-order electronic potentials shown in Fig. 2a; and  $\lambda$  is a coupling constant ( $\lambda = \xi/2$ , where  $\xi$  is the usual spin–orbit coupling parameter). Diagonalizing  $H(r)$  at each  $r$  gives the potential energy curves for the three electronic states of  $\text{I} \cdot \text{CO}_2$  including spin–orbit coupling. To quantify  $\lambda$ , we rely on the assumption (3) above and diagonalize  $H(r)$  in the limit of  $r \rightarrow \infty$ , that is with  $A_1(r) = B_1(r) = B_2(r) = 0$ . The eigenvalues ( $E_{1,2} = -\lambda$  and  $E_3 = 2\lambda$ ) correspond to the energy levels of isolated  $I({}^2P_{1/2,3/2})$ . From the known spin–orbit splitting in iodine (0.943 eV), we

determine  $\lambda = 0.314$  eV. We then diagonalize  $H(r)$  in Eq. (1) with this value of  $\lambda$  and obtain the  $\text{I} \cdot \text{CO}_2$  potentials shown in Fig. 2b. Note that  $\Omega$ , the projection of the electronic angular momentum on the molecular axis, used to label the electronic states of  $\text{I} \cdot \text{CO}_2$  in the pseudo-diatomic approximation [1–5,9–12], is not a good quantum number in the truly polyatomic description. In the absence of good quantum numbers, we label the states as *I*, *II*, and *III*.

To determine the significance of the  $C_{2v}$  description of the complex, we compare the potentials in Fig. 2b to those obtained in the pseudo-diatomic approximation. In that approximation, the non-degenerate  $B_1$  and  $B_2$  zero-order states merge into a degenerate  $\Pi$  state, whereas the  $A_1$  state correlates to a  $\Sigma$  state. The corresponding pseudo-diatomic potentials are shown in Fig. 2c, where the  $\Pi$  state potential [ $II(r)$ ] is obtained by averaging the  $B_1(r)$  and  $B_2(r)$  curves in Fig. 2a, and  $\Sigma(r) = A_1(r)$ .

The pseudo-diatomic Hamiltonian including spin–orbit coupling is obtained by substituting  $\Sigma(r)$  for  $A_1(r)$  and  $II(r)$  for both  $B_1(r)$  and  $B_2(r)$  in Eq. (1). The resulting Hamiltonian matrix can be directly diagonalized; however, it is instructive to follow the equivalent approach discussed by Hay and Dunning [9–12], and block-diagonalize it first. This procedure separates the states with different values of  $\Omega$  (with I–C as a quantization axis), yielding a  $2 \times 2$  matrix corresponding to two  $\Omega = 1/2$  states (labeled *I* 1/2 and *II* 1/2), and a single eigenvalue corresponding to the  $\Omega = 3/2$  (*I* 3/2) state:

$$H(r) = \begin{bmatrix} \Omega = 1/2 & & \\ \Sigma(r) & -\sqrt{2} \cdot \lambda & 0 \\ -\sqrt{2} \cdot \lambda & II(r) + \lambda & 0 \\ 0 & 0 & II(r) - \lambda \\ \Omega = 3/2 & & \end{bmatrix} \quad (2)$$

The *I* 3/2 state corresponds to the Hund's case (a)  ${}^2\Pi_{3/2}$  state, whereas the *I* 1/2 and *II* 1/2 states result from mixing of the Hund's case (a)  ${}^2\Pi_{1/2}$  and  ${}^2\Sigma$  states [1–5].

The *I* 3/2 state energy, as per Eq. (2), is  $II(r) - \lambda$ . The *I* 1/2 and *II* 1/2 state eigenvalues are determined by diagonalizing the  $\Omega = 1/2$  block at each value of  $r$ . The resulting pseudo-diatomic potentials of  $\text{I} \cdot \text{CO}_2$  are shown in Fig. 2d. Overall, these

potentials are similar to the  $C_{2v}$  potentials in Fig. 2b. However, a significant difference is observed for  $r < 4 \text{ \AA}$ : the *I* and *II*  $C_{2v}$  potentials never cross, whereas the *I*3/2 and *I*1/2 pseudo-diatomic curves intersect at  $r = 3.04 \text{ \AA}$ . This is clearly seen in Fig. 3 showing the (*II* – *I*) and (*I*3/2 – *I*1/2) difference potentials.

At short I–C distances, where the difference between the two models is observed, the spin–orbit coupling becomes increasingly a molecular property of the  $I \cdot CO_2$  complex. Therefore, we must examine the validity of treating the spin–orbit coupling as an atomic property of iodine. Table 1 lists I-atom spin densities for different zero-order ( $C_{2v}$ ) electronic states of  $I \cdot CO_2$  at selected C–I distances. It is instructive that the  ${}^2A_1$  state is most susceptible to spin delocalization, whereas in the  ${}^2B_1$  state the spin remains more than 99% localized on I, even at very short C–I distances (e.g.,  $r = 2.6 \text{ \AA}$ ). Attenuation of the spin by  $CO_2$  is maximized in the state with the greatest overlap of the half-filled I orbital with  $CO_2$  (the  $A_1$  state), and minimized in the state with the smallest overlap ( $B_1$ ). However, at distances relevant to our calculations ( $r > 3 \text{ \AA}$ ), at least 0.97 of the total spin density is localized on the I atom. Therefore, our explicit assumption about the atomic nature of spin–orbit coupling in  $I \cdot CO_2$  is sound.

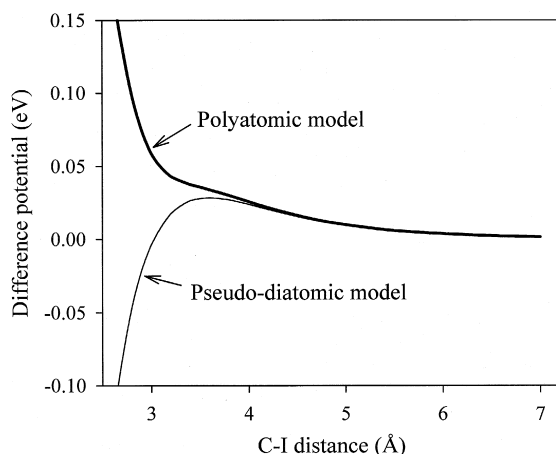


Fig. 3. The (*II* – *I*) and (*I*1/2–*I*3/2) difference potentials calculated for the polyatomic (*I*, *II*) and pseudo-diatomic (*I*1/2, *I*3/2) potentials of T-shaped  $I \cdot CO_2$  shown in Fig. 2b and d, respectively.

Table 1  
Mulliken spin density on the I atom in different zero-order ( $C_{2v}$ ) electronic states of  $I \cdot CO_2$  at selected C–I distances

C–I distance ( $\text{\AA}$ )	${}^2A_1$	${}^2B_1$	${}^2B_2$
7.0	1.000	1.000	1.000
6.0	0.999	1.000	1.000
5.0	0.998	1.000	1.001
4.0	0.996	1.000	1.001
3.6	0.991	1.000	1.002
3.3	0.982	1.000	1.001
3.0	0.968	0.999	0.997
2.8	0.953	0.996	0.989
2.6	0.930	0.991	0.976

Moreover, the atomic nature of spin–orbit coupling is assumed in both the  $C_{2v}$  and pseudo-diatomic models. Thus, the discrepancy between the two models is not due to this assumption and must result from the breakdown of the pseudo-diatomic approximation itself. The two difference potentials in Fig. 3 are nearly equal at  $r = 3.65 \text{ \AA}$ , corresponding to the calculated equilibrium distance in  $I^- \cdot CO_2$ , which explains why the pseudo-diatomic model is successful in describing the photoelectron spectrum [3–5]. At shorter I–C distances, relevant in even moderately energetic collisions, the pseudo-diatomic approximation becomes increasingly inadequate.

#### 4. $I \cdot OCS$ van der Waals complex

In this section, we consider the electronic structure of  $I \cdot OCS$  and  $I \cdot SCO$  linear complexes, and analyze the zero-order electronic structure of nonlinear  $I \cdot OCS$ . Fig. 1b shows possible orientations of the three 5p orbitals of the I atom relative to OCS. In the zero-order picture, both the  $I \cdot SCO$  and  $I \cdot OCS$  linear geometries correspond to either the  ${}^2\Sigma$  or degenerate  ${}^2\Pi$  electronic states. In the nonlinear geometry, the linear  $\Sigma$  state correlates with an  $A'$  state [denoted  $A'(\sigma)$ ], while the  $\Pi$  state gives rise to two distinct  $A'$  [denoted  $A'(\pi)$ ] and  $A''$  states.

Fig. 4a and c shows the zero-order potentials of linear  $I \cdot SCO$  and  $I \cdot OCS$ , respectively. Given the calculated equilibrium I–S distance in  $I^- \cdot SCO$  of  $3.6 \text{ \AA}$  [13], photodetachment of the anion places the neutral complex on the repulsive parts of both the  $\Sigma$  and  $\Pi$  potentials. As in  $I \cdot CO_2$ , the ordering of the

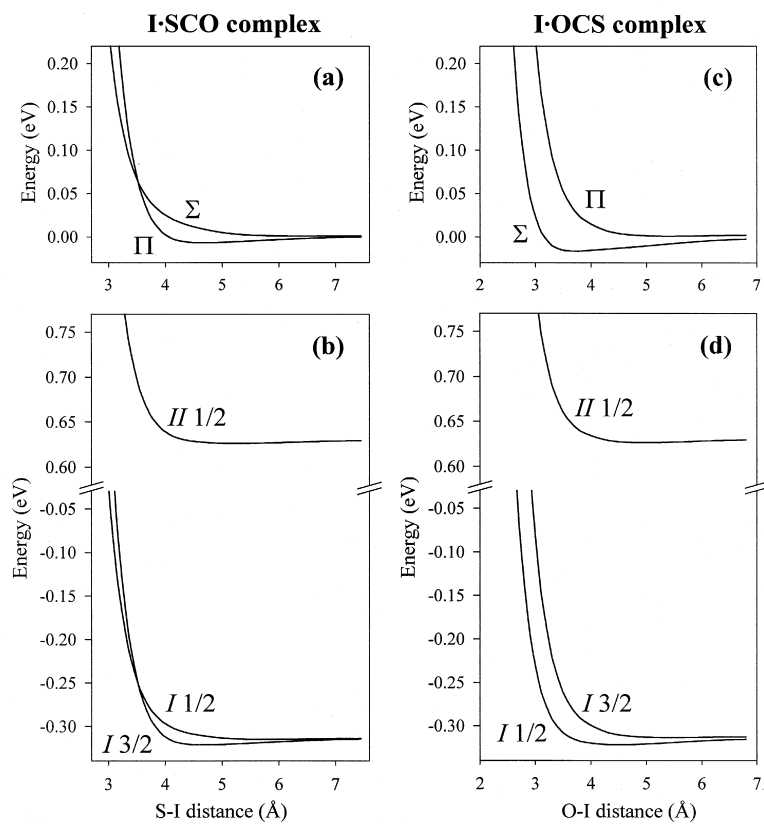


Fig. 4. (a) The  $\Sigma$  and  $\Pi$  zero-order electronic potentials of the linear  $I \cdot SCO$  complex. (b) Linear  $I \cdot SCO$  potentials including spin-orbit coupling. (c) The  $\Sigma$  and  $\Pi$  zero-order electronic potentials of the linear  $I \cdot OCS$  complex. (d) Linear  $I \cdot OCS$  potentials including spin-orbit coupling.

zero-order  $I \cdot SCO$  and  $I \cdot OCS$  states can be explained by considering the positive quadrupole moment associated with the hole on the I atom. In dipolar OCS, the S-end is slightly positive, while the O-end is negative. Therefore, a  $\sigma$  hole leads to repulsive interaction in  $I \cdot SCO$ , and attractive interaction in  $I \cdot OCS$ . On the other hand, a  $\pi$  hole implies that the  $\sigma$  orbital is occupied by two electrons, which interact attractively with the positive S-end of OCS and repulsively with the negative O-end. Thus, at moderate separations, the  $\Pi$  state of  $I \cdot SCO$  is lower in energy than the  $\Sigma$  state, with the order reversed for  $I \cdot OCS$ . Similar to  $I \cdot CO_2$ , the  $\Sigma$  state, in which the half-filled I-atom orbital is pointing towards OCS, is less repulsive at short I–S or I–O distances than the  $\Pi$  state. Because state ordering is sensitive to the electrostatic properties of the

solvent, the order of states is different in different van der Waals complexes, for example,  $I \cdot Ar$  and  $I \cdot CO_2$  ( $C_{2v}$ ) [4,22].

Since the energetic ordering of the  $\Sigma$  and  $\Pi$  states of linear  $I \cdot SCO$  and  $I \cdot OCS$  is different, several potential crossings occur at nonlinear geometries. Fig. 5 shows a correlation diagram, based on results of exploratory calculations in  $C_s$  symmetry, which reflects changes in the state order as a function of the I–OCS angle along the minimum energy path. The global zero-order potential minimum of  $I \cdot OCS$  corresponds to the  $A'(\pi)$  state. The equilibrium geometry is given by  $\theta = 110^\circ$  and  $r = 3.6 \text{ \AA}$ , where  $r$  is the distance from the OCS center of mass to the I atom, and  $\theta$  is the angle between the  $r$  vector and the SCO axis (e.g.,  $\theta = 0$  and  $180^\circ$  correspond to the linear  $I \cdot OCS$  and  $I \cdot SCO$  geometries,

respectively). At this minimum, the electronic dissociation energy of the complex is calculated to be 63 meV. A shallower minimum (dissociation energy 24 meV) exists on the  $A'(\sigma)$  surface, at  $\theta = 30^\circ$  and  $r = 4.8 \text{ \AA}$ , while the  $A''$  surface has its minimum at the linear  $I \cdot SCO$  geometry.

For the linear  $I \cdot SCO$  and  $I \cdot OCS$  geometries, we take into account the spin-orbit interaction by following the linear-molecule treatment of Hay and Dunning [9–12] discussed in Section 3. By diagonalizing the Hamiltonian matrix given by Eq. (2) with the zero-order  $\Sigma$  and  $\Pi$  potentials shown in Fig. 4a and c, we obtain the  $I \cdot SCO$  and  $I \cdot OCS$  potentials shown in Fig. 4b and d, respectively. As seen in Fig. 4b, the  $I3/2$  and  $I1/2$   $I \cdot SCO$  potentials intersect at an S–I distance of  $3.55 \text{ \AA}$  – approximately the same as the calculated equilibrium S–I<sup>-</sup> separation in  $I^- \cdot SCO$  [13]. Therefore, we predict that the contributions of the neutral  $I3/2$  and  $I1/2$  states to the photoelectron spectrum of the anion are overlapped.

Finally, we analyze the validity of treating the spin-orbit coupling in  $I \cdot OCS$  as an atomic property of iodine. Table 2 lists I-atom spin densities for the  $\Sigma$  and  $\Pi$  zero-order states of linear  $I \cdot SCO$  and  $I \cdot OCS$  at selected S–I and O–I distances, respectively. As in  $I \cdot CO_2$ , we find that the I-atom spin-density in the  $\Sigma$  state is more affected by the OCS than in the  $\Pi$  state, because of a greater overlap of

Table 2

Mulliken spin density on the I atom in different zero-order electronic states of linear  $I \cdot SCO$  and  $I \cdot OCS$  at selected S–I and O–I distances, respectively

I·SCO linear complex			I·OCS linear complex		
S–I distance ( $\text{\AA}$ )	$\Sigma$	$\Pi$	O–I distance ( $\text{\AA}$ )	$\Sigma$	$\Pi$
7.0	1.000	1.000	7.0	1.000	1.000
6.0	0.999	1.000	6.0	1.000	1.000
5.0	0.998	1.000	5.0	0.999	1.000
4.0	0.996	0.999	4.0	1.000	1.002
3.6	0.989	0.996	3.6	1.002	1.002
3.3	0.975	0.989	3.3	1.005	1.002
3.0	0.947	0.968	3.0	1.009	1.000
2.8	0.918	0.936	2.8	1.009	0.997

the corresponding half-filled orbital with OCS. We also find that spin delocalization is small at characteristic van der Waals distances. Therefore, the assumption about the atomic nature of spin-orbit coupling in  $I \cdot OCS$  and  $I \cdot SCO$  is sound.

## 5. Summary and conclusions

We have investigated theoretically the electronic structure of  $I \cdot CO_2$  and  $I \cdot OCS$  van der Waals complexes including spin-orbit interaction. For  $I \cdot CO_2$ , we emphasized one structural aspect that had not received adequate consideration in previous studies, i.e., the robustness of the pseudo-diatomic approximation in describing the T-shaped geometry of the complex. We compared the potentials calculated using both the pseudo-diatomic and truly polyatomic descriptions. At large I– $CO_2$  distances ( $> 4 \text{ \AA}$ ) the difference between the two models is negligible. At separations shorter than  $4 \text{ \AA}$ , the pseudo-diatomic approximation becomes increasingly invalid.

We calculated the potentials (including spin-orbit coupling) of linear  $I \cdot SCO$  and  $I \cdot OCS$ , and analyzed the zero-order electronic structure of nonlinear  $I \cdot OCS$ . We find that photodetachment of  $I^- \cdot SCO$  results in formation of the neutral complex on the repulsive parts of all neutral potentials, i.e., photodetachment is dissociative. We note that the photoelectron spectrum of  $I^- \cdot SCO$  is yet to be recorded.

Finally, we analyzed the validity of treating the spin-orbit interaction in  $I \cdot CO_2$  and  $I \cdot OCS$  as an

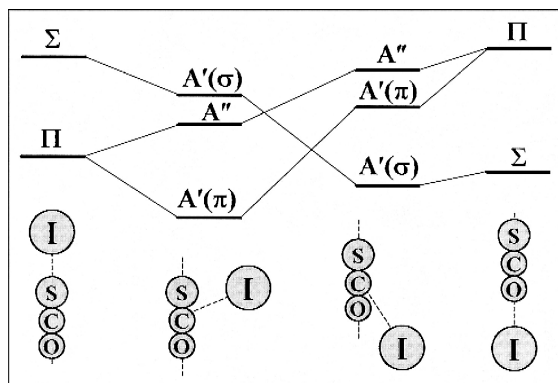


Fig. 5. A diagram connecting different zero-order electronic states of  $I \cdot OCS$  at both linear and nonlinear geometries along the minimum energy path from  $I \cdot SCO$  to  $I \cdot OCS$ . The diagram, based on the result of exploratory calculations in  $C_s$  symmetry, illustrates state ordering and potential crossings. See the text for details.

atomic property of iodine. We find this approximation justified at characteristic van der Waals separations, and more robust than the pseudo-diatomic approximation.

### Acknowledgements

The authors thank Professor Keiji Morokuma for helpful suggestions. This work was supported by the National Science Foundation.

### References

- [1] D.W. Arnold, S.E. Bradforth, E.H. Kim, D.M. Neumark, *J. Chem. Phys.* 102 (1995) 3493.
- [2] D.W. Arnold, S.E. Bradforth, E.H. Kim, D.M. Neumark, *J. Chem. Phys.* 102 (1995) 3510.
- [3] Y.X. Zhao, C.C. Arnold, D.M. Neumark, *J. Chem. Soc., Faraday Trans.* 89 (1993) 1449.
- [4] J. Faeder, N. Delaney, P.E. Maslen, R. Parson, *Chem. Phys.* 239 (1998) 525.
- [5] J. Faeder, Ph.D. Thesis, University of Colorado, Boulder, CO, 1998.
- [6] W.H. Breckenridge, *Acc. Chem. Res.* 22 (1989) 21.
- [7] W.H. Breckenridge, *Int. Rev. Phys. Chem.* 13 (1994) 291.
- [8] A.W.K. Leung, J.G. McCaffrey, W.H. Breckenridge, *J. Chem. Phys.* 109 (1998) 7777.
- [9] P.J. Hay, T.H. Dunning Jr., *J. Chem. Phys.* 66 (1977) 1306.
- [10] T.H. Dunning Jr., P.J. Hay, *Appl. Phys. Lett.* 28 (1976) 649.
- [11] T.H. Dunning Jr., P.J. Hay, *J. Chem. Phys.* 69 (1978) 134.
- [12] P.J. Hay, T.H. Dunning Jr., *J. Chem. Phys.* 69 (1978) 2209.
- [13] S. Nandi, A. Sanov, N. Delaney, J. Faeder, R. Parson, W.C. Lineberger, *J. Phys. Chem.* 102 (1998) 8827.
- [14] M.J. Frisch, G.W. Trucks, H.B. Schlegel, P.M.W. Gill, B.G. Johnson, M.A. Robb, J.R. Cheeseman, T. Kieth, G.A. Petersson, J.A. Montgomery, K. Raghavachari, M.A. Al-Laham, V.G. Zakrewski, J.V. Ortiz, J.B. Foresman, J. Cioslowski, B.B. Stefanov, A. Nanayakkara, M. Challacombe, C.Y. Peng, P.Y. Ayala, W. Chen, M.W. Wong, J.L. Andres, E.S. Replogle, R. Gomperts, R.L. Martin, D.J. Fox, J.S. Binkley, D.J. Defrees, J. Baker, J.P. Stewart, M. Head-Gordon, C. Gonzalez and J.A. Pople, *Gaussian 94*, Rev. E.1, Gaussian, Inc., Pittsburgh, PA, 1995.
- [15] A.D. Becke, *J. Chem. Phys.* 98 (1993) 5648.
- [16] C. Lee, W. Yang, R.G. Parr, *Phys. Rev. B* 37 (1988) 785.
- [17] W.R. Wadt, P.J. Hay, *J. Chem. Phys.* 82 (1985) 284.
- [18] M.N. Glukhovtsev, A. Pross, L. Radom, *J. Am. Chem. Soc.* 117 (1995) 2024.
- [19] T.H. Dunning Jr., *J. Chem. Phys.* 90 (1989) 1007.
- [20] R.A. Kendall, T.H. Dunning Jr., R.J. Harrison, *J. Chem. Phys.* 96 (1992) 6796.
- [21] D.E. Woon, T.H. Dunning Jr., *J. Chem. Phys.* 98 (1993) 1358.
- [22] J. Faeder, N. Delaney, P.E. Maslen, R. Parson, *Chem. Phys. Lett.* 270 (1997) 196.